To be submitted to *Journal of Physical Chemistry C*

# Silver ion mediated shape control of platinum nanoparticles: Removal of silver by selective etching leads to increased catalytic activity

Michael E. Grass, Yao Yue, Susan E. Habas, Robert M. Rioux[†], Chelsea I. Teall, and Gabor A. Somorjai*

Department of Chemistry, University of California, Berkeley and

Chemical Science Division, Lawrence Berkeley National Laboratory, Berkeley, CA 94720 USA

*email: somorjai@berkeley.edu

**RECEIVED DATE (to be automatically inserted after your manuscript is accepted if required according to the journal that you are submitting your paper to)**

[†]Present address: Department of Chemistry and Chemical Biology, Harvard University, Cambridge, MA 02144

A procedure has been developed for the selective etching of Ag from Pt nanoparticles of well-defined shape, resulting in the formation of elementally-pure Pt cubes, cuboctahedra, or octahedra, with a largest vertex-to-vertex distance of ~ 9.5 nm from Ag-modified Pt nanoparticles. A nitric acid etching process was applied Pt nanoparticles supported on mesoporous silica, as well as nanoparticles dispersed in aqueous solution. The characterization of the silica-supported particles by XRD, TEM, and $N_2$ adsorption measurements demonstrated that the structure of the nanoparticles and the mesoporous support remained conserved during etching in concentrated nitric acid. Both elemental analysis and ethylene hydrogenation indicated etching of Ag is only effective when $[HNO_3] \geq 7$ M; below this concentration, the removal of Ag is only ~ 10 %. Ethylene hydrogenation activity increased by four orders of magnitude after the etching of Pt octahedra that contained the highest fraction of silver. High-resolution transmission electron microscopy of the unsupported particles after etching demonstrated that etching does not alter the surface structure of the Pt nanoparticles. High $[HNO_3]$ led to the decomposition of the capping agent, polyvinylpyrollidone (PVP); infrared spectroscopy confirmed that many decomposition products were present on the surface during etching, including carbon monoxide.

KEYWORDS: Shape-controlled synthesis; Bimetallic nanoparticles; Silver etching; Platinum catalysis

## Introduction

Nanoparticles (NPs) synthesized by solution-phase methods are of interest for applications in catalysis, either as free particles in solution[1] or deposited on solid supports[2-4]. One area of interest in catalysis is the effect of NP shape on catalytic activity[5-10] and selectivity[11,12]. Many routes to shape-control of NPs have been explored, including control via ligand interactions[13-15], pH[5] or temperature[16], electrochemical routes[10,17], and the addition of other (sacrificial) metal ions[18-20] or NP seeds[21]. Shape control of NPs for catalysis is important because the particle shape determines which crystal faces are exposed[18] and the abundance of surface atoms with various metal coordination environments[22].

Previously we used $Ag^+$ ions to control the shape of Pt NPs[18] in an effort to elucidate how NP shape effects catalytic activity and selectivity[8]. Using this method, Pt cubes, cuboctahedra, or octahedra were synthesized with ≥ 80% selectivity for each shape by adding different concentrations of $AgNO_3$. Although initial results (X-ray diffraction and energy dispersive X-ray spectroscopy) indicated Ag was not present in the NPs after removing excess AgCl, it was later found that residual Ag of up to ~ 20 at %, is still present in the NP system (metal NP plus stabilizing polymer). In a subsequent paper, we found that Ag acts as a poison in the hydrogenation of ethylene by Pt and the amount of Ag in the NPs can be directly correlated to the decrease in catalytic activity. This is in agreement with studies of highly dispersed Pt-Ag catalysts on silica gel; in that study, rates of 1-hexene hydrogenation decreased exponentially with increasing Ag content[23].

In this paper, we present the post-synthesis etching of Ag from Pt NPs synthesized in the presence of $AgNO_3$, and their subsequent use as hydrogenation

catalysts. Nitric acid etching of Ag is a well-studied system because of its use in the synthesis of $AgNO_3$ from elemental silver[24]. The dependence of etching on temperature, $HNO_3$ concentration, and silver particle size (mm-range) is well-documented[24-27]. The reaction proceeds with the overall stoichiometry at $HNO_3$ concentrations between 3.8 and 4.9 M:

$$4HNO_3(aq) + 3Ag(s) \rightarrow 3AgNO_3(aq) + NO(g) + 2H_2O(l) \quad [1]$$

For [$HNO_3$] of 4.9 – 7.1 M, the stoichiometry is

$$2HNO_3(aq) + Ag(s) \rightarrow AgNO_3(aq) + NO_2(g) + H_2O(l) \quad [2]$$

Platinum, on the other hand, is resistant to etching by nitric acid, usually being dissolved with aqua regia (70 % concentrated hydrochloric acid and 30 % concentrated nitric acid). Using this difference in reactivity towards nitric acid, we are able to modify the Pt-Ag NPs after synthesis to pure platinum nanoparticles of well-defined shapes.

Post-synthetic chemical modification of nanoparticles has previously been used to develop nanostructures with a variety of properties. For example, Chen *et al.* synthesized Pd-Ag and Pt-Ag nanoboxes using galvanic replacement of Ag from Ag nanocubes with $Na_2PdCl_4$ or $Na_2PtCl_6$[20]. The surface plasmon resonance peak of these nanoboxes could be tuned across the entire visual spectrum by this approach. In another report from this group, Au nanoboxes and nanoframes were formed by dealloying Au/Ag nanoboxes using an aqueous etchent[28]. Post-synthetic etching of bimetallic nanostructures is a new tool of nanotechnology with the potential to yield new and structures with novel applications.

## Experimental

### *2.1 Nanoparticle synthesis*

A detailed description of the synthesis of the NPs has been published elsewhere[18]. A brief description is given here. The synthesis of Pt cubes began with the introduction of 0.5 ml of 2 mM silver nitrate ($AgNO_3$, 99+%, Sigma-Aldrich) solution in ethylene glycol (EG, min. 98%, EMD) to boiling EG (3 ml); followed by the immediate introduction of 3 ml of poly(vinylpyrrolidone) (PVP, MW = 55 K, Sigma-Aldrich, 375 mM) and 1.5 ml of hexachloroplatinic acid ($H_2PtCl_6 \cdot 6H_2O$, 99.9%, metals basis, Alfa-Aesar, 62.5 mM) EG solutions over 16 minutes by the injection of small aliquots every 30 seconds. The resulting mixture was heated at reflux for an additional five minutes, cooled, and precipitated with acetone. The solid was collected by centrifugation and redispersed in ethanol. Insoluble AgCl in this solution was removed by centrifugation and the supernatant was precipitated with hexanes and again dispersed in ethanol. Increasing the molarity of the $AgNO_3$ solution to 20 mM and 60 mM led to the selective formation of cuboctahedral and octahedral particles, respectively. The synthesis was was conducted at the exact same conditions, but without the addition of $AgNO_3$.

### *2.2 Catalyst Synthesis*

A detailed procedure for the synthesis of catalysts by NP encapsulation (NE) in high surface-area mesoporous silica can be found elsewhere[3]. After a second precipitation with hexanes, the NPs were dispersed in 23.7 ml of an aqueous triblock co-polymer solution (Pluronic P123, $EO_{20}PO_{70}EO_{20}$, EO = ethylene oxide, PO = propylene oxide, BASF, 750 mg) and stirred for 1 h at 313 K, followed by the quick addition of an aqueous solution (114 µl) of 0.5 M sodium fluoride (NaF, 99.99%, Aldrich) and 1.2 ml of

tetramethyl orthosilicate (TMOS, 98%, Aldrich) to the reaction mixture, and stirred for one day at 313 K. The resulting slurry was aged for an additional day at 373 K in a closed vessel. After filtering and washing the brown precipitate with water and ethanol, the catalyst was dried in a convection oven at 373 K overnight.

*2.3 Etching*

*2.3.1 Etching of Pt(shape)/SBA-15 Catalysts*

Silver was etched from the supported Pt(shape)/SBA-15 catalysts with nitric acid solutions (EMD Nitric Acid, 15.7 M) at 333 ± 2 K for 0.5 h with stirring. After etching, the catalysts were filtered with a large excess of water, rinsed in ethanol and dried at 373 K overnight. The stock 15.7 M $HNO_3$ solution was diluted with deionized water to various concentrations to examine the influence of [$HNO_3$] on etching. A note of caution with this etching procedure: $NO_2$ forms during the etching process and concentrated $HNO_3$ is very corrosive.

*2.3.2 Etching of Unsupported Particles*

The etching of unsupported Pt NP's was similar to the supported catalyst samples. A sample of Pt NPs containing ~1 mg Pt was dispersed in water, and $HNO_3$ was added to obtain the desired concentration. After stirring at 333 K for 0.5 h, the particles were precipitated with acetone, centrifuged, and redispersed in ethanol. Prior to IR measurements (discussed below), the Pt NP sols were precipitated with hexane and redispersed in ethanol, as described previously, an additional three times to remove excess PVP and to ensure there was no residual $HNO_3$. A note of caution with this etching procedure: $NO_2$ forms during the etching process and concentrated $HNO_3$ is very corrosive.

*2.4 Characterization of Pt/SBA-15 Catalysts.*

*2.4.1 Physical and Chemical Characterization.*

Transmission electron microscopy (TEM) experiments were carried out on a Philips/FEI Tecnai 12 microscope operated at 100 kV at the Robert D. Ogg Electron Microscope Laboratory at the University of California, Berkeley. Catalysts were sonicated in acetone for 10 s, dropped on continuous carbon film coated copper grids (Ted Pella), and dried in air. The unsupported NPs diluted with ethanol were treated similarily. High-resolution TEM (HRTEM) experiments were carried out on a Phillips CM200/FEG operated at 200 kV at the National Center for Electron Microscopy (NCEM) at the Lawrence Berkeley National Laboratory. X-ray diffraction (XRD) patterns were measured on a Bruker D8 GADDS diffractometer using Co $K_\alpha$ radiation ($\lambda$ = 1.79 Å). Elemental analyses for Pt and Ag by inductively coupled plasma optical emission spectroscopy (ICP-OES) was performed at Galbraith Laboratories, Inc. (Knoxville, TN.).

*2.4.2 Diffuse Reflectance Infrared Study of CO Adsorption on Pt/SBA-15 Catalysts*

*In-situ* diffuse-reflectance infrared Fourier transform spectroscopy (DRIFTS) was used to study the adsorption of CO on Pt(octahedra)/SBA-15 catalysts. Experiments were conducted with a Nicolet Nexus 670 spectrometer equipped with a Thermo Spectra-Tech controlled atmosphere-diffuse reflection cell. Samples (~10 mg) of unetched and etched catalysts were calcined at 673 K *ex-situ* in a tube furnace, followed by an *in-situ* reduction at 573 K in 10 % $H_2$/He at 30 $cm^3$ (NTP) $min^{-1}$. A single-beam spectrum (2 $cm^{-1}$ resolution, scan number of 128) of the freshly reduced catalyst was obtained at 300 K under 30 $cm^3$ (NTP) He $min^{-1}$ and used as the background for spectra taken of the same

catalyst in the presence and absence of gas-phase CO at 300 K. Samples were exposed to a 30 $cm^3$ (NTP) $min^{-1}$ mixture of 10 % CO/He for 0.5 h at 300 K, followed by purging in 30 $cm^3$ (NTP) He $min^{-1}$ at 300 K. The spectra reported here are taken while purging with He.

*2.4.3 Attenuated Total Reflection (ATR) Infrared Studies of CO adsorption*

After synthesis and etching of shape controlled Pt NPs containing Ag as well as particles synthesized in the absence of Ag, the NPs were precipitated with acetone, centrifuged, and the supernatant was discarded. The NPs were then washed by dispersing them in ethanol and then precipitating them with hexanes four times, and finally they were dispersed in 200 μl ethanol to obtain a concentrated NP sol. Attenuated total reflection Fourier transform infrared (ATR-FTIR) (Nicolete Avatar 360) spectra were taken after placing five drops (~50 μl) of the ethanol NP sol onto a ZnSe ATR crystal drop by drop, allowing the previous drop to dry before the application of the next drop. All spectra were obtained by averaging 8 scans at 2 $cm^{-1}$ resolution.

*2.5 Catalytic Reaction Studies of Ethylene Hydrogenation*

Catalytic reactions were studied in a Pyrex plug U-tube flow reactor connected to a ¼" stainless steel manifold containing mass flow controllers (Unit Instruments) for delivery of reactant gases. Ethylene (AirGas, CP grade), hydrogen (Praxair, UHP, 99.999%) and helium (Praxair, UHP, 99.999%) were used as-received. Reaction temperatures were measured with a thermocouple extending into the catalyst bed supported on a quartz frit. Ethylene and ethane were detected by gas chromatography (Hewlett Packard 5890) using a homemade $Al_2O_3$ column (15 ft. length, 1/8" diameter). Reaction rate measurements were conducted at differential conditions (all conversions

were < 10%). Typically the catalyst (1 – 40 mg) was diluted with low-surface area, acid-washed quartz in a 1:5 w/w ratio (catalyst:quartz).

## Results and Discussion

*3.0 Summary of Previous Results from this System and Motivation for Current Study*

The initial work on the synthesis of these Pt NPs focused on obtaining shape control of Pt NPs of less than 10 nm and was accomplished through the addition of $AgNO_3$ into the reaction mixture[18]. With increasing the $AgNO_3$ concentration, Pt cubes, cuboctahedra, and octahedra were formed, each with > 80 % selectivity. It was concluded that Ag was absent in the NPs after the ethanol/hexanes washing, based on the absence of a Ag peak in the energy dispersive X-ray spectrum for washed Pt(octahedra) as well as the absence of diffraction peaks corresponding to Ag or any shift in the Pt diffraction peaks[18]. Later, high-resolution (synchotron-based) XRD confirmed there was no formation of a Pt-Ag alloy in the Pt(octahedra) (Figure S1). Further single particle electron dispersive X-ray (EDX) studies, however, indicated that up to ~ 15 at % Ag remained in the Pt(octahedra) after washing.

In an effort to study the effect of NP faceting on catalysis, the three NP shapes were loaded onto SBA-15 and their activity for ethylene hydrogenation was measured[8]. In this study, ICP-OES elemental analysis indicated that for samples of Pt(cubes)/SBA-15, Pt(cuboctahedra)/SBA-15, and Pt(octahedra)/SBA-15, Ag comprises 1.4 %, 9.5 %, and 11.5 % of the total metal, respectively. The catalytic activity scaled with the amount of Ag in the catalysts; the turnover frequencies (TOF) (in $s^{-1}$) for Pt(cubes)/SBA-15, Pt(cuboctahedra)/SBA-15, and Pt(octahedra)/SBA-15 were 8.6, 0.4, and 0.02,

respectively. In contrast, the turnover frequencies for Pt(111) and Pt(100) single crystals are 9.3 $s^{-1}$ and 3.6 $s^{-1}$ for the same reaction conditions[29]. Thus, it was concluded that the Ag content, not the NP faceting, was responsible for the change in TOF.

The results of these two studies motivated us to develop a method for the removal of Ag from the Pt(cubes), Pt(cuboctahedra), and Pt(octahedra) NPs. In this study, we demonstrate that Ag can be removed from the NPs without loss of shape, and that after Ag removal, the TOF for ethylene hydrogenation is comparable to the TOF for a similarly prepared Pt(no Ag) catalyst.

*3.1 Nanoparticle Synthesis*

The slow addition of separate PVP and $H_2PtCl_6 \bullet 6H_2O$ solutions to boiling EG caused the color of the solution to change from yellow to dark brown, indicating the fast reduction of Pt(IV) to Pt(0). If Ag ions were not added prior to the introduction of the Pt salt, a distribution of Pt particle shapes were obtained, dominated by cubes with rounded corners[18]. The addition of varying concentrations of $AgNO_3$ effectively modifies the growth rates along the <111> and <100> directions to give shape control of the Pt NPs. At a $AgNO_3$ concentration of 1.1 mol % (relative to Pt salt concentration), cubes formed with ~ 80 % selectivity, while at 11 % and 32 mol % $AgNO_3$, cuboctahedra and octahedra formed with ~ 100 % and 80 % selectivity, respectively. In the case of the cubes and octahedra syntheses, the minor shape is tetrahedral. For all NPs, the largest vertex-to-vertex distance is ~ 9.5 nm regardless of shape with a dispersion in size of ~ 7 %. Cubes and octahedra are terminated entirely by (100) and (111) planes, respectively, while cuboctahedra are terminated by six (100) and eight (111) surfaces. UV–Vis absorption spectroscopy indicated the presence of reduced $Ag_4^{2+}$ species during the early

stages of synthesis, with the formation of AgCl particles at longer synthesis times in the case of the octahedra[18]. It is believed that the mechanism for Pt NP growth involves enhanced growth along the <100> and/or suppressed growth along <111> directions due to the introduction of Ag ions and their strong adsorption on {100} terminated Pt surfaces. Silver can be removed from Pt octahedra by repetitive centrifugation and redispersion after Pt particle formation as determined by UV–Vis spectroscopy[18] and elemental analysis (Table 1 – Pt(octahedra) are synthesized with 32 mol % Ag). However, ICP-OES elemental analysis performed in this study suggests that little, if any, silver is removed from Pt cubes or cuboctahedra by centrifugation (Table 1 – Pt(cuboctahedra) and Pt(cubes) are synthesized with 10.7 and 1.1 mol % Ag respectively).

*3.2 Catalyst Synthesis*

After purifying the Pt NPs, they were introduced into an aqueous solution of Pluronic P123 triblock co-polymer at 313 K and stirred for 1 h to ensure complete dispersion of the Pt particles. Brown precipitates formed within five minutes of the addition of 0.5 M NaF and TMOS. The supernatant was colorless and transparent, indicating the Pt colloids incorporated into or on the surface of the silica matrix. Particles are often found in groups, but the particles within these groups do not appear to be in contact. Low resolution TEM does not indicate any change in particle shape after encapsulation, but HRTEM analysis (necessary to determine the surface structure) is difficult due to encapsulation of the particles within the SBA-15 matrix. Particle sizes determined by XRD before and after encapsulation are in good agreement, and no aggregation of particles was observed[3].

*3.3 Etching*

*3.3.1 Etching of Supported Nanoparticles*

Platinum NPs were incorporated into SBA-15 and used to study the effect of [$HNO_3$] etching on the particles. The majority of the data presented here involves Pt(octahedra)/SBA-15 catalysts for which the mol % Ag, $Ag^+/(Pt^{4+} + Ag^+)$, used for the synthesis of these NPs is 32.0 %. After ethanol/hexanes washing and loading onto SBA-15, this decreased to 12 – 16 mol % Ag (Table 1). This indicated that about half of the Ag used in the synthesis of the Pt NPs is removed by centrifugation of insoluble AgCl[18]. For both the Pt(cubes) and Pt(octahedra), the amount of silver present in the supported catalysts is the same as the amount of Ag used in the synthesis. The amount of platinum and silver remaining in the Pt(octahedra)/SBA-15 catalyst after etching with 0, 1, 6, 8, and 10 M $HNO_3$ is listed in Table 1, along with the amounts of platinum and silver found in the Pt(cubes)/SBA-15 and Pt(cuboctahedra)/SBA-15 samples before and after etching with 10 M $HNO_3$. A Pt(no Ag)/SBA-15 catalyst synthesized without any $AgNO_3$ and a second Pt(octahedra)/SBA-15 catalysts are also included for comparison. The amount of Ag remaining in the Pt(octahedra)/SBA-15 catalysts decreased by 10 % relative to Pt after a 1 M etch and 16 % after etching in 6 M $HNO_3$. After etching the catalyst in 8 M $HNO_3$, > 84 % of the Ag was removed and increasing [$HNO_3$] had no apparent effect. It appears that a small amount of the silver etched easily, but significant etching of silver requires [$HNO_3$] > 7 M.

There are many possibilities for the 7 M threshold for significant Ag etching. One possibility is that most of the Ag only reacts with $HNO_3$ through the high [$HNO_3$]

mechanism (eq. 2) due to interactions of Ag or $HNO_3$ with Pt or PVP. In a study by Balbaud *et al.*, the reduction of $HNO_3$ at a Pt electrode, the catalytic decomposition produces NO, but not $NO_2$ in 4 M $HNO_3$, while for 8 M and 12 M $HNO_3$, the formation of $NO_2$ is observed[30]. The formation of $NO_2$ in this study is inferred from the evolution of a yellow-orange gas during etching at high nitric acid concentrations (> 6 M), in agreement with the electrochemical studies by Balbaud. This clear change in mechanism for $HNO_3$ reduction over platinum with increasing [$HNO_3$] may be responsible for the Ag etching observations.

Etching in nitric acid does not result in aggregation of the NPs supported on SBA-15 or destruction of the SBA-15 structure or pores (Figures 1 and S2). The Pt crystallite sizes decreases by ~ 20 % after etching with 15 M $HNO_3$ (Figure 2), although loss of Pt is ruled out by ICP-OES analysis (Table 1). The calculated XRD particle size (calculated using the Scherrer equation) for the unetched Pt(octahedra)/SBA-15 catalyst was 9.3 nm which decreased to 9.0 nm, 8.5 nm, 8.6 nm, and 8.1 nm after etching with 1 M, 4 M, 7 M, and 15 M nitric acid, respectively. The largest change in crystallite size (1.2 nm) corresponds to a ~ 6 Å shell, or ~ 3 atomic layers. XRD provided no insight into the origin of the crystallite size decrease, but infrared studies suggest some possibilities (section *3.4.3*).

*3.3.2 Etching of Unsupported Nanoparticles*

We conducted the same etching procedure on unsupported Pt NPs. The NPs after thorough washing were dispersed in water, followed by the addition of the appropriate amount of concentrated nitric acid. During these etching experiments, orange

discoloration of the caps and sides of the scintillation vial was observed for [$HNO_3$] > 6 M, indicating $NO_2$ formation during the etching procedure.

TEM images indicated no change in particle shape or size, but the aggregation between particles increased (Figure 3). The aggregation was also apparent by eye; for samples etched with [$HNO_3$] ≤ 4 M, the NP sol remained homogeneous, while a dark brown precipitate formed after a 10 M etch, and etching with 13 M $HNO_3$ caused the particles to precipitate completely, leaving a clear supernatant. This aggregation is probably a result of the degradation of PVP, which normally prevents particle agglomeration[31] (section *3.4.3*). Figure 4 shows HRTEM images of the as-synthesized platinum cubes and octahedra and after etching with 10 M nitric acid. There does not appear to be any significant structural change for the Pt(cubes) or pt(octahedra) NPs. Therefore, we consider this post-synthetic ething step as a method to clean Pt NPs with well-defined surface morphologies even though shape control required the presence of a second metal. This method should be suitable for any Pt-metal (M) system, in which an etchant selectively etches M over Pt.

*3.4.2 DRIFTS Study of CO Adsorption on Pt/SBA-15 Catalysts*

After calcination and *in-situ* reduction, we exposed the catalyst to flowing CO, and purged with He. After completely purging the diffuse reflectance cell, we recorded FTIR spectra. Figure 5 shows the spectra recorded for a Pt(octahedra)/SBA-15 catalyst. A peak at 2084 $cm^{-1}$ appeared for samples etched in 4 M or 15 M $HNO_3$, but is absent for the unetched catalyst and the catalyst etched in 1 M $HNO_3$. This peak is indicative of atop CO bound to platinum and was not observed for nude SBA-15 or in the samples with high Ag content. No CO bands are observed for 0 M and 1 M samples, and we

therefore concluded that more CO binds to the particles etched with at least 4 M $HNO_3$. Silver appears to block the adsorption of CO by these catalysts either by physical site blocking or altering the electronic structure of the Pt surface, or both (further discussion in section *3.4.4*).

*3.4.3 Attenuated Total Reflection Infrared Studies*

The etching process was investigated using ATR-FTIR of unsupported Pt(No Ag), Pt(cubes) and Pt(cuboctahedra) (Figure 6). There are five peaks of interest in the infrared spectrum, belonging to different carbonyl species. The peak at 1653 $cm^{-1}$ is due to the carbonyl stretch of PVP for unbound monomers as observed in the FTIR spectrum of pure PVP. The intensity of this peak can be understood from the 12:1 (PVP monomer):Pt ratio used for NP synthesis. At a slightly lower energy (~1597 $cm^{-1}$), a peak is present in the ATR-FTIR spectrum of the etched Pt cubes but not seen in the spectrum of the unetched particles. This peak has previously been assigned to the carbonyl stretch of PVP for a monomer coordinated to the Pt surface using surface enhanced Raman spectroscopy (SERS)[32]. Bridge bound NO on Pt[33] also has a stretching frequency of 1600 $cm^{-1}$, and this assignment cannot be ruled out. The ratio of the unbound to the bound PVP carbonyl peak decreased with increasing [$HNO_3$], and we attributed the relative increase in intensity to the degradation of PVP, causing an increase in the relative intensity of the peak at 1597 $cm^{-1}$ compared to that at 1653 $cm^{-1}$. The peaks at 2026 $cm^{-1}$, and 1815 $cm^{-1}$ are consistent with atop and bridge bound CO, respectively[34]. Both peaks are red-shifted compared to gas phase studies[34], but it is difficult to make direct comparisons due to the complex surface chemistry of these samples. The peak observed at 2130 $cm^{-1}$ might be a product of the decomposition of

PVP by $HNO_3$. During the reaction between NO and CO on supported Pt catalysts, peaks at 2130 – 2150 $cm^{-1}$ were attributed to surface intermediates[35]. In the case of a $Pt/SiO_2$ catalyst, a peak at 2142 $cm^{-1}$ was assigned to either a platinum fulminate (Pt-CNO), cyanate (Pt-OCN), or isocyanate (Pt-NCO)[35]. In a study by Unland, et al. with $Pt/Al_2O_3$, a peak at 2130 $cm^{-1}$ was attributed to cyanate ion while a peak at 2261 $cm^{-1}$ was assigned to covalently-bound isocyanate[36]. Similarly, in the case of the reaction between $NO_2$ and propene over $Pt/Al_2O_3$, strong peaks were observed at 2254 $cm^{-1}$, 2232 $cm^{-1}$, and 2141 $cm^{-1}$. The first two peaks were assigned to bound isocyanate, consistent with Unland's analysis, but the 2141 $cm^{-1}$ band was assigned as a C-N stretch of surface cyanide (Pt-CN)[37]. It is difficult to ascertain the exact source of each peak because of the complex nature of the system under study, but their presence does suggested PVP decomposition in acidic solution occurs with the concurrent formation of numerous surface-bound decomposition products.

The gas-phase stretching frequency for CO bound to polycrystalline Ag and large $Ag_n$ clusters ($n > 280$) appears at 2110 $cm^{-1}$, shifting to lower wavenumbers with decreasing particle size, 2080 $cm^{-1}$ for $Ag_{30}$ clusters[38]. The frequency for CO bound to $Ag^+$ cations on $SiO_2$ is 2169 $cm^{-1}$ and the CO is weakly bound, desorbing with room temperature evacuation[39]. Assignment of peaks to CO bound to Ag or $Ag^+$ has been ruled out based on the similarity between FTIR-ATR spectra from NPs synthesized with and without Ag (Figure 6).

*3.5 Ethylene Hydrogenation on Unetched and Etched Pt(shape)/SBA-15*

Ethylene hydrogenation is a very sensitive probe of active sites on a Pt catalyst. Under the reaction conditions used in this study (10 Torr $C_2H_4$, 200 Torr $H_2$, 295 K), the

turnover frequency is ~ 20 $s^{-1}$ on supported Pt catalysts, Pt single crystals, and other "model" Pt catalysts, but is nearly completely poisoned by the presence of silver on the surface[8]. For this reason, ethylene hydrogenation was used as a probe of Pt active sites exposed as a result of Ag etching by $HNO_3$. In all of the figures, the TOF is determined by estimating the number of surface Pt atoms from TEM measurements, which were in good agreement with XRD. Figure 7 shows the TOF (log scale) and Ag content for a Pt(octahedra)/SBA-15 catalyst etched in nitric acid solutions between 0 and 15.7 M. From this plot, it is clear that Ag is etched efficiently from the Pt NPs when $[HNO_3] > 7$ M and that ethylene hydrogenation is extremely sensitive to the amount of Ag in the Pt catalysts. At $[HNO_3] > 7$ M, there is very little change in [Ag] or the TOF for ethylene hydrogenation.

Multiple samples of Pt(octahedra)/SBA-15, Pt(cuboctahedra)/SBA-15, Pt(cubes)/SBA-15, and Pt(no Ag)/SBA-15 were prepared and etched in various concentrations in order to further understand the relationship between the content and activity for ethylene hydrogenation. as well as to see if the $[HNO_3]$ plays a role in affecting $C_2H_4$ TOF beyond Ag etching. Figure 8 presents all of this data together with data from ref. 8 on similar samples in a plot of $TOF/TOF_{MAX}$ vs. $Ag/Pt_s$, where $TOF_{MAX}$ (34 $s^{-1}$) is the turnover frequency measured for a Pt(no Ag)/SBA-15 catalyst and $Pt_s$ is the estimated number of surface atoms from TEM measurements. The turnover frequency depended exponentially on the $Ag/Pt_s$ ratio. If Ag poisoned the Pt catalyst through a physical site blocking mechanism, the dependence of the rate on the amount of silver on the surface would be linear, but instead we observed an exponential dependence:

$$TOF/TOF_{MAX} = 0.88\exp\left(-6.15\times\left(Ag/Pt_s\right)\right) \qquad [3]$$

This suggests there is an electronic component to the poisoning of Pt towards ethylene hydrogenation by Ag, which has been previously observed for Pt-Ag bimetallic catalysts in the hydrogenation of 1-hexene[23]. In that work, however, Pt-Ag alloy particle were shown to form, and the activity for 1-hexene hydrogenation correlated well with the lattice parameter of the alloy.

It is possible that the Ag in this case forms a surface alloy with Pt, but a bulk alloy has been ruled out by high-resolution XRD (Figure S1). The bulk phase diagram for Pt-Ag indicates that alloying does not occur at low temperatures (< 1100 K)[40]. Röder *et al.* found that when Ag is deposited on Pt(111) at room temperature, a Ag layer forms that is one atom thick, but when Ag is deposited at 620 K (or the surface is annealed at 620 K after room temperature deposition), it dissolves into the Pt surface layer and forms islands[41]. This surface segregation of Ag on Pt(111) has also been shown in a theoretical study[42]. The picture of alloying between Pt and Ag is not so clear, and studies have shown that phase diagrams for alloys can change with particle size[43]. In two separate X-ray absorption fine structure (XAFS) studies, no alloying was observed for a Pt-Ag catalyst, even for particle sizes down to 2 nm[44,45]. Pt-Ag bimetallic NP systems have produced Pt(core)/Ag(shell)[46] and also Ag(core)/Pt(shell)[47] structures as indicated by UV-Vis spectroscopy combined with modeling based on Mie theory. On the other hand, alloying in Pt-Ag bimetallic NP systems has been observed by employing XRD[23] or a combination of XRD, HRTEM, and UV-Vis spectroscopy[48]. In each of these studies, the synthetic conditions were different and thus it is difficult to draw any general conclusions about alloying in Pt-Ag nanoscale systems.

An alternate explanation, in addition to site blocking or surface alloying, for the decrease in TOF is decreased electron density in the Pt 5d orbital due to a Pt(5d) → Ag charge transfer. This charge transfer was proposed in the case of Ag on Pt(111) where no alloying occurred[49]. Additionally, all samples fit this trend despite the different etching concentrations used to achieve the same Ag content, indicating that the observed effect is dominated by Ag content rather than an ancillary effect of $HNO_3$ etching. The etched Pt(shape)/SBA-15 catalysts hydrogenate ethylene at the same rate as a catalyst synthesized without silver, demonstrating that nitric acid etching can effectively remove Ag to produce pure Pt NPs.

**Conclusions**

Silver can be selectively removed from shape-controlled platinum nanoparticles either before or after deposition on a silica support by etching with concentrated nitric acid (≤ 15.7 M) at 333 K. The shape -- cubic, cuboctahedral, or octahedral -- and size of the particles remained unchanged after etching as determined by X-ray diffraction, transmission electron microscopy, and high-resolution transmission electron microscopy. The etching of platinum nanoparticles suspended in solution leads to severe aggregation when the nitric acid concentration is greater than 10 M, an outcome of the decomposition of the stabilizing polymer, poly(vinylpyrrolidone), as monitored by attenuated total reflection infrared spectroscopy. Elemental analysis for silver demonstrated the complete etching of silver from platinum catalysts at nitric acid concentrations greater than 7 M with no evidence of platinum etching. Ethylene hydrogenation was very sensitive to the silver content in silica-supported Pt catalysts and depended exponentially on the $Ag:Pt_s$

ratio. These results confirm that Ag using in the synthesis of shape-controlled Pt nanoparticles is confined to the surface.

**Acknowledgements.** This work was supported by the Director, Office of Science, Office of Advanced Scientific Computing Research, Office of Basic Energy Sciences, Chemical Sciences, Geosciences, and Biosciences Division, of the U.S. Department of Energy under Contract No. DE-AC02-05CH11231. The Advanced Light Source is supported by the Director, Office of Science, Office of Basic Energy Sciences, of the U.S. Department of Energy under Contract No. DE-AC02-05CH11231. R. M. R. acknowledges the Ford Motor Company for financial support through a graduate fellowship administered by the Berkeley Catalysis Center. We thank the National Center for Electron Microscopy at the Lawrence Berkeley National Laboratory and the Robert D. Ogg Electron Microscope Lab at UC Berkeley for use of their facilities. We also thank Professor Robert G. Bergman for use of the ATR-FTIR spectrometer, Professor A. Paul Alivisatos for use of the X-ray diffractometer, and Professor Peidong Yang for helpful discussions.

**Supporting Information Available:** The supporting information contains high resolution XRD spectra of Pt(No Ag) and Pt(octahedra) NPs, $N_2$ adsorption isotherms for an unetched and etched Pt(octahedra)/SBA-15 catalyst, and time-on-stream plots of ethylene hydrogenation TOF for an unetched and etched Pt(octahedra)/SBA-15 catalyst. This material is available free of charge via the Internet at http://pubs.acs.org.

FIGURE CAPTIONS

**Figure 1.** TEM images of Pt(octahedra)/SBA-15 (a) before etching and (b) after 10 M $HNO_3$ etch. The micrographs demonstrate both the nanoparticles and support are visually unchanged by the etching procedure and the nanoparticles tend to cluster in groups, but do not aggregate after treatment – in oxygen or hydrogen – at temperatures between 373 and 573 K.

**Figure 2.** XRD data of Pt(octahedra)/SBA-15 (a) as-synthesized, and after etching with [$HNO_3$] of (b) 1 M, (c) 4 M, (d) 7 M, and (e) 15 M. The crystallite size is measured from the FWHM of the 111 peak, which broadens slightly with increasing $HNO_3$ etching concentration. The lines (A) and (B) are the bulk Ag 111 and Pt 111 diffraction peaks, respectively.

**Figure 3.** TEM images of Pt(octahedra) (a) as-synthesized, and after etching with [$HNO_3$] of (b) 1 M, (c) 7 M, and (d) 13 M. The etching of nanoparticles in increasing [$HNO_3$] lead to the decomposition of the PVP surface-protecting layer leading to nanoparticle aggregation in solution. At a concentration of 15 M, the particles completely precipitate out of solution leaving a clear supernatant.

**Figure 4.** HRTEM images of Pt(cube) (a) before etching and (b) after 10 M etch and Pt(octahedra) (c) before etching and (d) after 10 M etch.

**Figure 5.** Infrared (DRIFTS) spectra of CO adsorbed on Pt(octahedra)/SBA-15 at 295 K (a) as synthesized, and after etching with [$HNO_3$] of (b) 1 M, (c) 4 M, and (d) 15 M. CO

adsorption on Pt is not observed until [$HNO_3$] is ~ 4 M, and the intensity of atop-bound CO increases with etching at higher [$HNO_3$]. A peak position of 2090 $cm^{-1}$ is in good agreement with single-crystal observations[34] and a calcined-reduced Pt(7.1 nm)/SBA-15 catalyst[3].

**Figure 6**. Infrared (FTIR-ATR) spectra of (I) Pt(no Ag), (II) Pt(cube), and (III) Pt(cuboctahedra) (a) as synthesized, and after etching with [$HNO_3$] of (b) 1 M, (c) 6 M, (d) 7 M, and (e) 15 M. All magnified sections of the spectra (1700 – 2300 $cm^{-1}$) are magnified 5×.

**Figure 7.** Ethylene hydrogenation TOF and silver content of Pt(octahedra)/SBA-15 after various $HNO_3$ etching treatments. The reported rate is the initial TOF at 10 Torr ethylene and 200 Torr hydrogen in balance He. The etching of Ag and the ethylene hydrogenation rates are dramatically enhanced when [$HNO_3$] > 7 M.

**Figure 8**. Initial ethylene hydrogenation TOF (10 Torr ethylene and 200 Torr hydrogen in balance He) for Pt(No Ag)/SBA-15 (●), Pt(cubes)/SBA-15 (□), Pt(cuboctahedra)/SBA-15 (▲), and Pt(octahedra)/SBA-15 (◇) as a fraction of the TOF for a Pt(No Ag)/SBA-15 catalyst ( $TOF/TOF_{MAX} = TOF/TOF_{Pt(No\ Ag)/SBA\text{-}15} = TOF/34\ s^{-1}$ ) before and after $HNO_3$ etching with [$HNO_3$]. The TOF ratio is plotted versus the ratio of Ag atoms to surface Pt atoms ($Pt_s$). Three points in this graph are taken from earlier work[6]. All turnover frequencies are reported at standard conditions of 10 Torr ethylene and 200 Torr hydrogen in balance He.

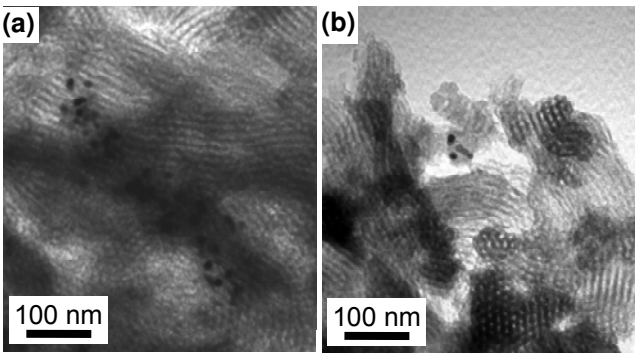


Figure 1

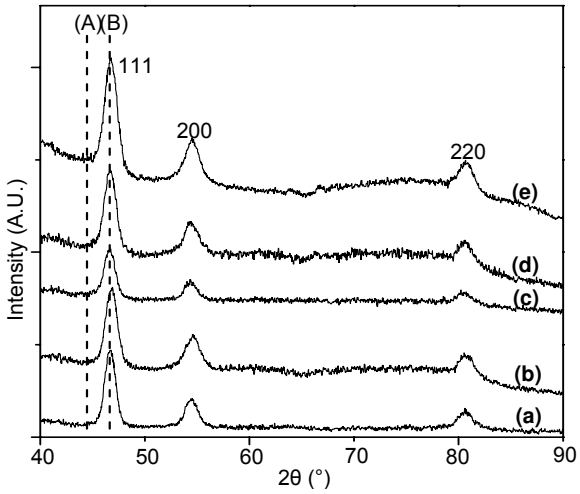


Figure 2

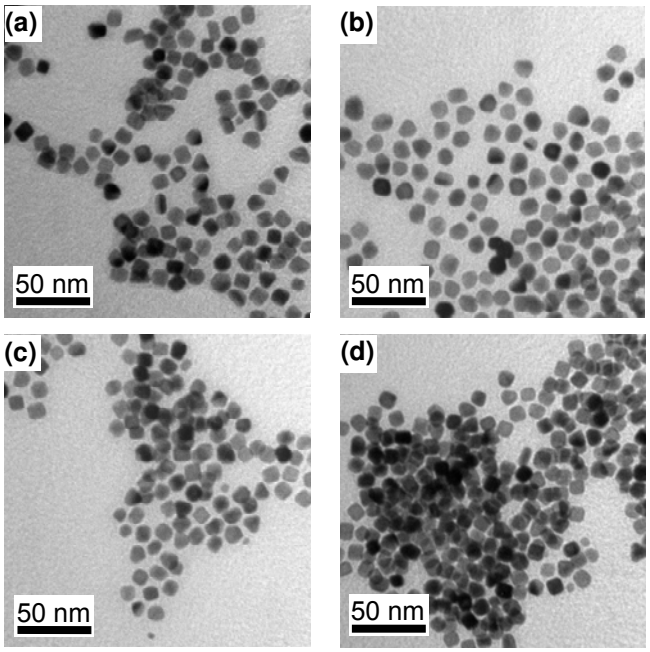


Figure 3

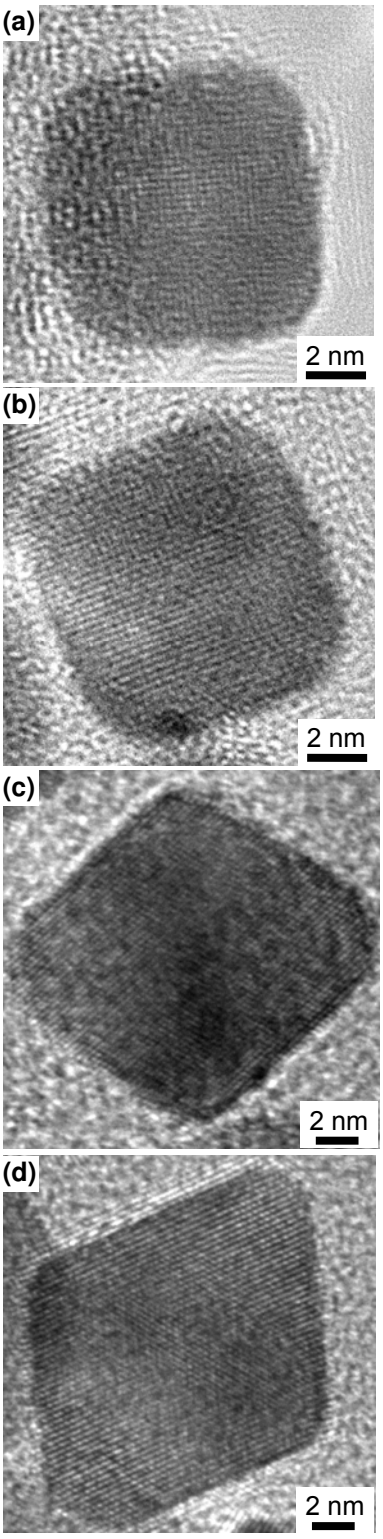


Figure 4

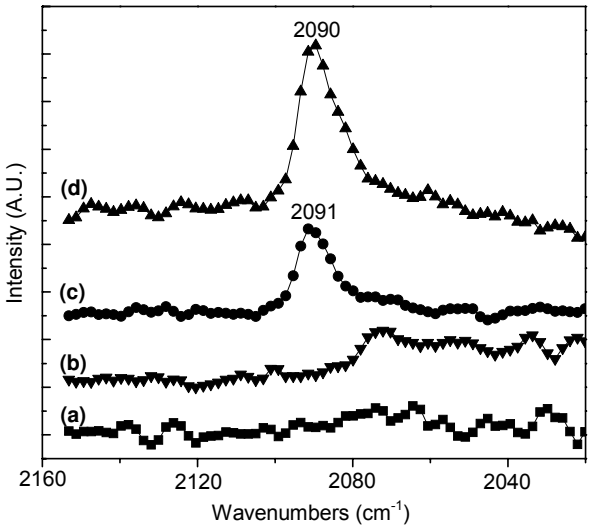
2090
2091
(d)
(c)
(b)
(a)
Intensity (A.U.)
2160
2120
2080
2040
Wavenumbers (cm-1)

Figure 5

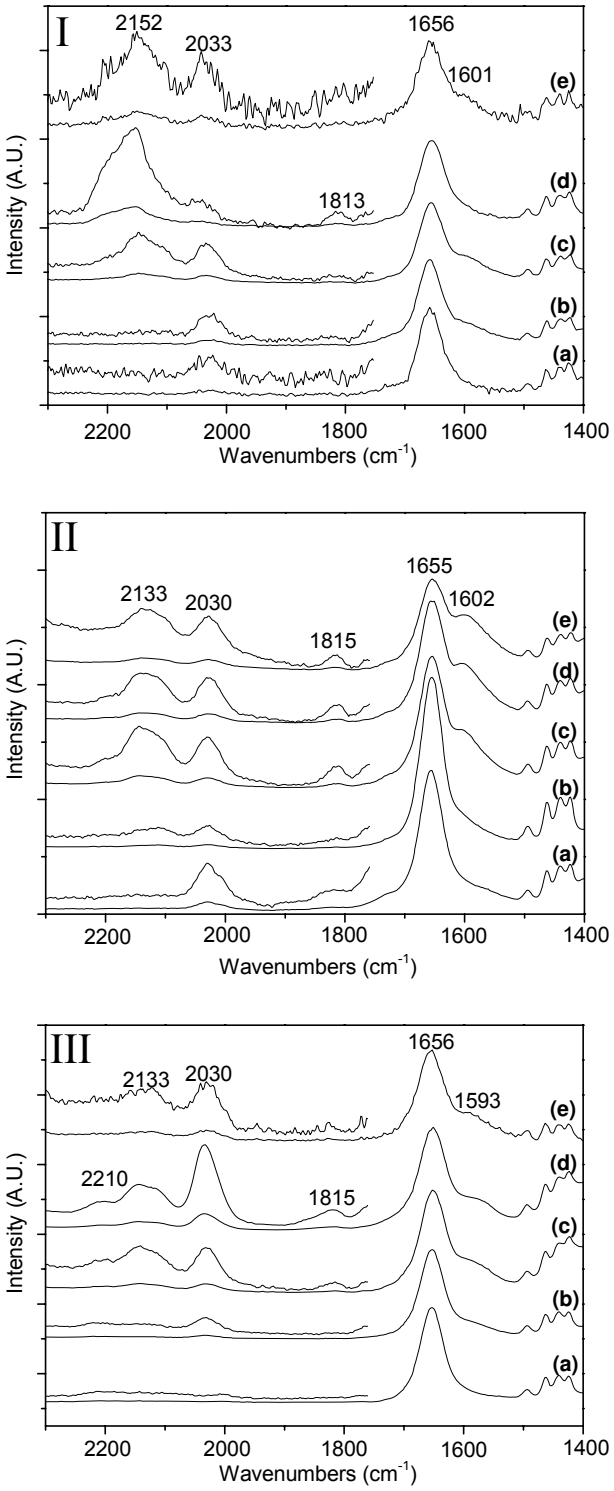
I
2152
2033
1656
1601
(e)
1813
(d)
(c)
(b)
(a)
Intensity (A.U.)
2200
2000
1800
1600
1400
Wavenumbers (cm-1)
II
1655
2133
2030
1602
(e)
1815
(d)
(c)
(b)
(a)
Intensity (A.U.)
2200
2000
1800
1600
1400
Wavenumbers (cm-1)
III
1656
2133
2030
1593
(e)
(d)
2210
1815
(c)
(b)
(a)
Intensity (A.U.)
2200
2000
1800
1600
1400
Wavenumbers (cm-1)

Figure 6

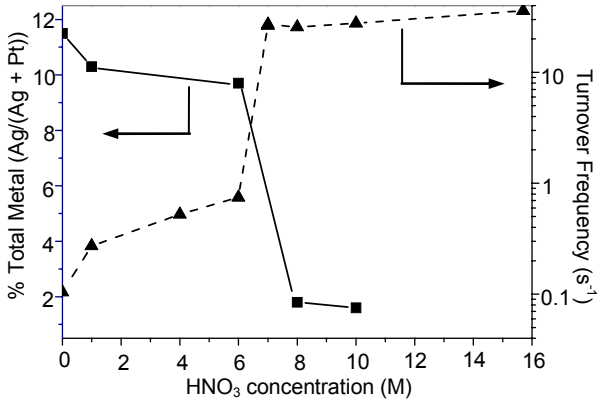
% Total Metal (Ag/(Ag + Pt))
Turnover Frequency (s-1)
HNO3 concentration (M)
12
10
8
6
4
2
0
2
4
6
8
10
12
14
16
10
1
0.1

Figure 7

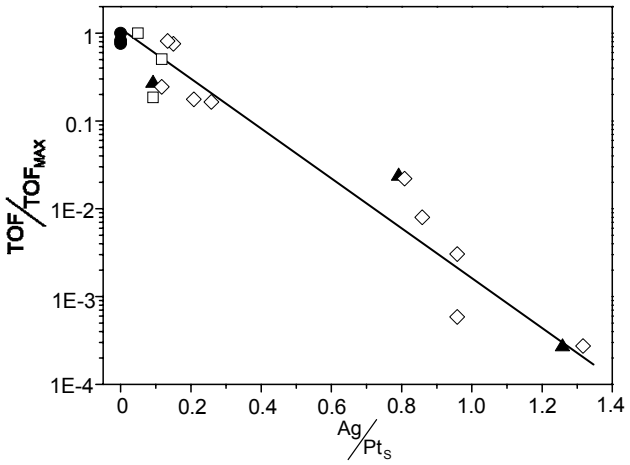


Figure 8

TABLES

**Table 1. ICP-OES elemental analysis of PVP-protected Pt NP catalysts before and after nitric acid etching treatments**

| sample | $[HNO_3]$ (M)[a] | % Pt[b] | ppm Ag[b] | Ag/(Pt+Ag)×$10^2$ [c] | % Ag remaining |
|---|---|---|---|---|---|
| Pt(No Ag)/SBA-15[d] | 0 | 0.67 | < 56 | < 1.4 | -- |
| Pt(cube)/SBA-15 | 0 | 0.83 | < 53 | < 1.1 | -- |
| | 10 | 0.82 | < 27 | < 0.59 | -- |
| Pt(cuboctahedra)/SBA-15 | 0 | 0.65 | 544 | 15.1 | -- |
| | 10 | 0.66 | < 42 | < 1.1 | < 7.3 |
| Pt(octahedra)/SBA-15 | 0 | 0.76 | 500 | 11.5 | -- |
| | 1 | 0.85 | 489 | 10.3 | 89.6 |
| | 6 | 0.86 | 466 | 9.7 | 84.3 |
| | 8 | 0.84 | 82 | 1.8 | 15.7 |
| | 10 | 0.86 | < 76 | < 1.6 | < 13.9 |
| Pt(octahedra)/SBA-15 #2[e] | 0 | 0.85 | 748 | 15.8 | -- |
| | 10 | 0.82 | < 62 | < 1.4 | < 8.9 |

[a] Catalyst etching performed at 333 K with stirring for 30 min in a nitric acid with the indicated concentration
[b] Determined by ICP-OES
[c] Represents the mole percent of total metal that is Ag
[d] Sample prepared without silver as reference. Pt precursor is 99.9% pure, so the Ag content of this sample is assumed to be the detection limit under these conditions.
[e] Sample was prepared by the same method

References

(1) Roucoux, A.; Schulz, J.; Patin, H. *Chem. Rev.* **2002**, *102*, 3757.

(2) Rioux, R. M.; Song, H.; Hoefelmeyer, J. D.; Yang, P.; Somorjai, G. A. *J. Phys. Chem. B* **2005**, *109*, 2192.

(3) Song, H.; Rioux, R. M.; Hoefelmeyer, J. D.; Komor, R.; Niesz, K.; Grass, M.; Yang, P. D.; Somorjai, G. A. *J. Am. Chem. Soc.* **2006**, *128*, 3027.

(4) Gupta, G.; Stowell, C. A.; Patel, M. N.; Gao, X. X.; Yacaman, M. J.; Korgel, B. A.; Johnston, K. P. *Chem. Mater.* **2006**, *18*, 6239.

(5) Lee, H.; Habas, S. E.; Kweskin, S.; Butcher, D.; Somorjai, G. A.; Yang, P. D. *Angew. Chem. Int. Ed.* **2006**, *45*, 7824.

(6) Miyazaki, A.; Balint, I.; Nakano, Y. *J. Nanopart. Res.* **2003**, *5*, 69.

(7) Narayanan, R.; El-Sayed, M. A. *Nano Lett.* **2004**, *4*, 1343.

(8) Rioux, R. M.; Song, H.; Grass, M.; Habas, S.; Niesz, K.; Hoefelmeyer, J. D.; Yang, P.; Somorjai, G. A. *Top. Catal.* **2006**, *39*, 167.

(9) Telkar, M. M.; Rode, C. V.; Chaudhari, R. V.; Joshi, S. S.; Nalawade, A. M. *Appl. Catal., A* **2004**, *273*, 11.

(10) Tian, N.; Zhou, Z. Y.; Sun, S. G.; Ding, Y.; Wang, Z. L. *Science* **2007**, *316*, 732.

(11) Xu, R.; Wang, D. S.; Zhang, J. T.; Li, Y. D. *Chem. Asian J.* **2006**, *1*, 888.

(12) Chimentao, R. J.; Kirm, I.; Medina, F.; Rodriguez, X.; Cesteros, Y.; Salagre, P.; Sueiras, J. E.; Fierro, J. L. G. *Appl. Surf. Sci.* **2005**, *252*, 793.

(13) Ahmadi, T. S.; Wang, Z. L.; Green, T. C.; Henglein, A.; El-Sayed, M. A. *Science* **1996**, *272*, 1924.

(14) Bakshi, M. S.; Kaura, A.; Bhandari, P.; Kaur, G.; Torigoe, K.; Esumi, K. *J. Nanosci. Nanotechnol.* **2006**, *6*, 1405.

(15) Kim, F.; Connor, S.; Song, H.; Kuykendall, T.; Yang, P. D. *Angew. Chem. Int. Ed.* **2004**, *43*, 3673.

(16) Hoefelmeyer, J. D.; Niesz, K.; Somorjai, G. A.; Tilley, T. D. *Nano Lett.* **2005**, *5*, 435.

(17) Sun, J. L.; Zhang, J. H.; Liu, W.; Liu, S.; Sun, H. S.; Jiang, K. L.; Li, Q. Q.; Guo, J. H. *Nanotechnology* **2005**, *16*, 2412.

(18) Song, H.; Kim, F.; Connor, S.; Somorjai, G. A.; Yang, P. D. *J. Phys. Chem. B* **2005**, *109*, 188.

(19) Seo, D.; Park, J. C.; Song, H. *J. Am. Chem. Soc.* **2006**, *128*, 14863.

(20) Chen, J. Y.; Wiley, B.; McLellan, J.; Xiong, Y. J.; Li, Z. Y.; Xia, Y. N. *Nano Lett.* **2005**, *5*, 2058.

(21) Xu, Z. C.; Shen, C. M.; Xiao, C. W.; Yang, T. Z.; Zhang, H. R.; Li, J. Q.; Li, H. L.; Gao, H. J. *Nanotechnology* **2007**, *18*.

(22) Van Hardeveld, R.; Hartog, F. *Surf. Sci.* **1969**, *15*, 189.

(23) Campostrini, R.; Giovanni, C.; Dire, S.; Scardi, P. *J. Mol. Catal.* **1989**, *53*, L13.

(24) Martinez, L., Segarra, M., Fernandez, M., Espiell, F. *Metall. Trans. B* **1993**, *24B*, 827.

(25) Ozmetin, C., Copur, M., Yartasi, A., Kocakerim, M.M. *Chem. Eng. Technol.* **2000**, *23*, 707.

(26) Ozmetin, C., Copur, M., Yartasi, A., Kocakerim, M.M. *Ind. Eng. Chem. Res.* **1998**, *37*, 4641.

(27) Bancroft, W. D. *J. Chem. Soc.* **1924**, *28*, 973.

(28) Lu, X. M.; Au, L.; McLellan, J.; Li, Z. Y.; Marquez, M.; Xia, Y. N. *Nano Lett.* **2007**, *7*, 1764.

(29) Backman, A. L.; Masel, R. I. *J. Vac. Sci. Technol., A* **1988**, *6*, 1137.

(30) Balbaud, F.; Sanchez, G.; Santarini, G.; Picard, G. *Eur. J. Inorg. Chem.* **2000**, 665.

(31) Napper, D. H. *Polymeric Stabilization of Colloidal Dispersions*; Academic Press: London, 1983.

(32) Borodko, Y.; Humphrey, S. M.; Tilley, T. D.; Frei, H.; Somorjai, G. A. *J. Phys. Chem. C* **2007**, *111*, 6288.

(33) Dejong, K. P.; Meima, G. R.; Geus, J. W. *Appl. Surf. Sci.* **1982**, *14*, 73.

(34) Somorjai, G. A. *Introduction to Surface Chemistry and Catalysis*; Wiley-Interscience: New York, 1994.

(35) Anderson, J. A.; Rochester, C. H. *J. Chem. Soc., Faraday Trans.* **1991**, *87*, 1485.

(36) Unland, M. L. *J. Phys. Chem.* **1973**, *77*, 1952.

(37) Bamwenda, G. R.; Ogata, A.; Obuchi, A.; Oi, J.; Mizuno, K.; Skrzypek, J. *Appl. Catal., B* **1995**, *6*, 311.

(38) Froben, F. W.; Rabin, i.; Ritz, M.; Schulze, W. *Z. Phys. D: At., Mol. Clusters* **1996**, *38*, 335.

(39) Hadjiivanov, K.; Knozinger, H. *J. Phys. Chem. B* **1998**, *102*, 10936.

(40) Okamoto, H. *J. Phase Equilib. Diffus.* **1997**, *18*, 485.

(41) Roder, H.; Schuster, R.; Brune, H.; Kern, K. *Phys. Rev. Lett.* **1993**, *71*, 2086.

(42) Christensen, A.; Ruban, A. V.; Stoltze, P.; Jacobsen, K. W.; Skriver, H. L.; Norskov, J. K.; Besenbacher, F. *Phys. Rev. B* **1997**, *56*, 5822.

(43) Yasuda, H.; Mori, H. *J. Cryst. Growth* **2002**, *237*, 234.

(44) Lahiri, D.; Bunker, B.; Mishra, B.; Zhang, Z. Y.; Meisel, D.; Doudna, C. M.; Bertino, M. F.; Blum, F. D.; Tokuhiro, A. T.; Chattopadhyay, S.; Shibata, T.; Terry, J. *J. Appl. Phys.* **2005**, *97*.

(45) Doudna, C. M.; Bertino, M. F.; Blum, F. D.; Tokuhiro, A. T.; Lahiri-Dey, D.; Chattopadhyay, S.; Terry, J. *J. Phys. Chem. B* **2003**, *107*, 2966.

(46) Henglein, A. *Langmuir* **2001**, *17*, 2329.

(47) Lizmarzan, L. M.; Philipse, A. P. *J. Phys. Chem.* **1995**, *99*, 15120.

(48) Torigoe, K.; Nakajima, Y.; Esumi, K. *J. Phys. Chem.* **1993**, *97*, 8304.

(49) Rodriguez, J. A.; Kuhn, M. *J. Phys. Chem.* **1994**, *98*, 11251.

TOC ARTWORK